Rheological Properties of Cement Mortar with Fly Ash and Silica Fume for 3D Printing

Israa Alhanafy[1*], Salah Altoubat[1], M Talha Junaid[1], Mohamed Maalej[1], and Matěj Prudil[2]

[1]University of Sharjah, United Arab Emirates
[2]Brno University of Technology, Czech Republic

Keywords: 3D printing; rheology; fly ash; silica fume; cement mortar; flow curve.

Abstract. This study examines the rheological behavior of cement-based mortar mixes designed for 3D printing by varying fly ash (FA) and silica fume (SF) contents and testing at different resting times. Six mixes were prepared: three with 0%, 15%, and 30% FA at a 0.30 water-to-binder (w/b) ratio, and three with 0%, 10%, and 20% SF at a 0.45 w/b ratio. Anton Paar MCR 302 rheometer was used to perform a standard hysteresis loop test to measure static yield stress, dynamic yield stress, plastic viscosity, and thixotropy at 0, 15, and 30 minutes after mixing. Results showed that the 15% fly ash mix developed notably high static and dynamic yield stresses along with the greatest thixotropy at later resting times, implying a beneficial balance of flowability and structural build-up. In contrast, the 30% fly ash mix showed a significant drop in both yield stress and thixotropy after 30 minutes. This suggests it required excessive water and that the pozzolanic reaction was slower. For silica fume mixes, the 20% SF mix had the highest yield stresses overall. However, the 10% SF mix achieved better thixotropy at 30 minutes. These findings support ongoing efforts to create mix designs that improve pumpability, extrudability, and layer stability for additive manufacturing in construction.

1. Introduction

Additive manufacturing (AM), or 3D printing, has reshaped many industries by allowing complex objects to be built layer by layer directly from digital designs. The advantages of AM are reduced material waste, automation, and significant savings in both time and cost have made it a game-changing technology for design and manufacturing [1, 4]. Among its many uses, three-dimensional concrete printing (3DCP) has gained attention in the construction industry for its potential to simplify labor-intensive tasks and reduce material usage. However, successful use of 3DCP depends heavily on achieving the right rheological properties, such as yield stress, viscosity, and thixotropy. These properties are critical for making the mixture pumpable, extrudable, and stable enough to support successive layers. Supplementary cementitious materials (SCMs) like fly ash (FA) and silica fume (SF) , along with resting time, significantly impact these properties. Fly ash is often used in 3DCP for its ability to improve flowability. It can enhance pumpability by reducing internal friction, leading to reductions in both static and dynamic yield stresses at moderate replacement levels [5–8]. However, extremely high levels of fly ash may cause a slight increase in yield stress over time. This could be due to secondary hydration or interactions within the cement paste [9]. Silica fume, due to its ultrafine nature, acts both as a filler to enhance particle packing and as a pozzolanic material that contributes to early strength development. Several studies show that adding a small percentage of silica fume (e.g., 2–2.5%) substantially increases yield stress and thixotropy [7, 10], thereby enhancing buildability—but excessive amounts risk stiffening the mix to the point of restricting flow and pumpability [11, 12]. Resting time—covering any delay between mixing and printing or between successive layers—further influences rheological evolution, since ongoing hydration and flocculation processes progressively increase yield stress and thixotropy [13, 14]. While short rest intervals may lead to insufficient structural build-up and layer deformation, prolonged delays can produce excessively stiff material that is difficult to extrude [15, 16]. Numerical data indicate, for example, that yield stress can drop from 500 Pa to 300 Pa when 30% fly ash replaces cement, and the flow diameter in slump tests may increase by 15% at 50% fly ash content, thereby improving pumpability and extrusion suitability [17]. Silica fume, on the other hand, increases viscosity and promotes better cohesion and structural build-up because of the ultrafine particle size and its high surface area. Adding 6–12% silica fume, for instance, has been shown to raise the dynamic yield stress from 300 Pa to 650 Pa and the viscosity from 12 Pa·s to 25 Pa·s [18]. Combined, fly ash and silica fume can balance flowability and buildability: a mix incorporating 50% fly ash and 10% silica fume has been shown to

* Corresponding author: u22200131@sharjah.ac.ae

produce consistent rheological properties (yield stress of around 450–550 Pa and viscosity of 20–30 Pa·s) ideal for extrusion-based printing [19]. Furthermore, regarding thixotropy—which is vital for layer-by-layer stability—fly ash tends to reduce the thixotropic index (facilitating smoother extrusion), whereas silica fume raises it (enhancing post-extrusion resistance to deformation) [10]. Recent advancements in 3D printing technology have significantly enhanced its applicability in the construction industry. For example, researchers have been working on automated systems that help minimize waste and improve efficiency, offering promising alternatives to traditional construction methods [20, 21]. However, scaling up 3D printing for larger projects remains a challenge. Address the practical challenges that arise when these technologies are used on construction sites is still needed [22, 23]. One of the key issues is optimizing material flow to ensure smooth printing while maintaining structural stability. Advances in SCMs have played an important role in overcoming these challenges. Recent research has focused on improving layer bonding and enhancing the flow behavior of cement-based mixtures. By incorporating superplasticizers and admixtures, researchers can better control factors like yield stress, viscosity, and thixotropy [24, 25]. These improvements have made it possible to develop high-performance, 3D-printable concrete mixes tailored to meet the demands of different construction applications.

The main aim of the research is to systematically study and improve the flow behavior of cement-based mortars designed for 3D printing by changing the amounts of FA and SF. This study aims to understand how these SCMs affect important flow properties such as static and dynamic yield stress, viscosity, and thixotropy. By targeting these properties, researchers aim to improve the performance of 3D-printed construction materials, improving their pumpability, ease of extrusion, and layer stability. These developments contribute to ongoing efforts to improve 3D printing for large-scale and sustainable construction.

2. Methods

Six concrete mixes were prepared to assess how FA and SF affect the flow properties of 3D-printable mortar at various water-to-binder (w/b) ratios, as shown in Table 1. The main binder was Ordinary Portland Cement (OPC, ASTM Type I), along with Class F fly ash (ASTM C618 compliant) and Grade 920D silica fume, both obtained from local suppliers in the UAE. Mixes were prepared and tested under controlled conditions of 25 ± 2°C temperature. The fine aggregate content (0–2 mm) and a fixed 2% superplasticizer dosage (by total binder mass) were kept constant across all mixes. To investigate the role of FA in improving workability without requiring additional water, three mixes (0%, 15%, and 30% FA replacement of OPC) were produced at a 0.30 w/b ratio. Similarly, to address SF's higher water demand and prevent overly stiff mixtures, another three mixes (0%, 10%, and 20% SF replacement) were prepared at a 0.45 w/b ratio. To ensure consistency in the fine aggregates particle size distribution used in the concrete mixes, a sieve analysis was conducted. The fine aggregates were sieved through standard sieves ranging from 2 mm to 0.075 mm to determine the percentage passing through each sieve. The resulting distribution of the particle size is shown in Fig. 1. All samples were prepared following the step by step procedure [26] outlined in Table 2.

Table 1. Mix Design Details

ID	w/b[1]	SP%[2]	s/b[3]	SF%	FA%
FA0	0.3	2%	1	0	0
FA15					15
FA30					30
SF0	0.45			0	0
SF10				10	
SF20				20	

[1] w/b: water-to-binder ratio.
[2] SP%: percentage of superplasticizer by total binder mass.
[3] s/b: sand-to-binder ratio

The following procedure, outlined in Table 2, were used to prepare the mixtures. For the rheometer test, one batch is made for each mix then three different specimens were tested at intervals of 0, 15, and 30 minutes after mixing. The rheological properties, including thixotropy, viscosity, and yield stresses, were measured using a standard hysteresis loop test performed with an Anton Paar MCR 302 rheometer with a 50 mm parallel plate spindle. The gap between the plates was set to 4 mm, and tests were performed within a shear rate range of 0 to 100 s^{-1}. Yield stress and viscosity were determined using the Bingham model. A single shear history method was employed, generating a hysteresis loop by recording the up-curve and down-curve (Fig. 2(a)). During testing, the spindle's rotational speed was increased from 0 s^{-1} to 100 s^{-1} over 60 seconds and then reduced back to 0 s^{-1} in another 60 seconds.

Yield stress and plastic viscosity were calculated from the down-curve (shear rate range of 20 s^{-1} to 80 s^{-1}) using the Bingham equation presented in Eq. 1:

$$\tau = \tau_0 + \eta\gamma^{\cdot} \tag{1}$$

where τ is the shear stress, τ_0 is the yield stress, η is the plastic viscosity, and $\gamma^{\cdot}$ is the shear rate. Thixotropy was quantified by calculating the enclosed area between the up-curve and down-curve (Fig. 2(b)), representing the energy stored in the flocculated structure of the sample.

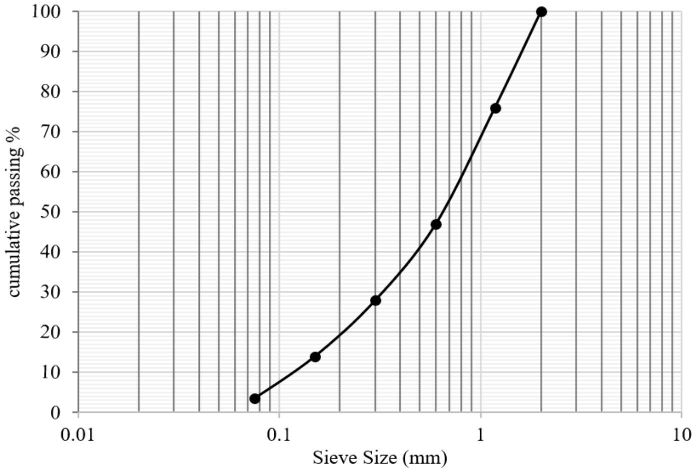

Fig. 1. The sieve analysis of the fine aggregates used.

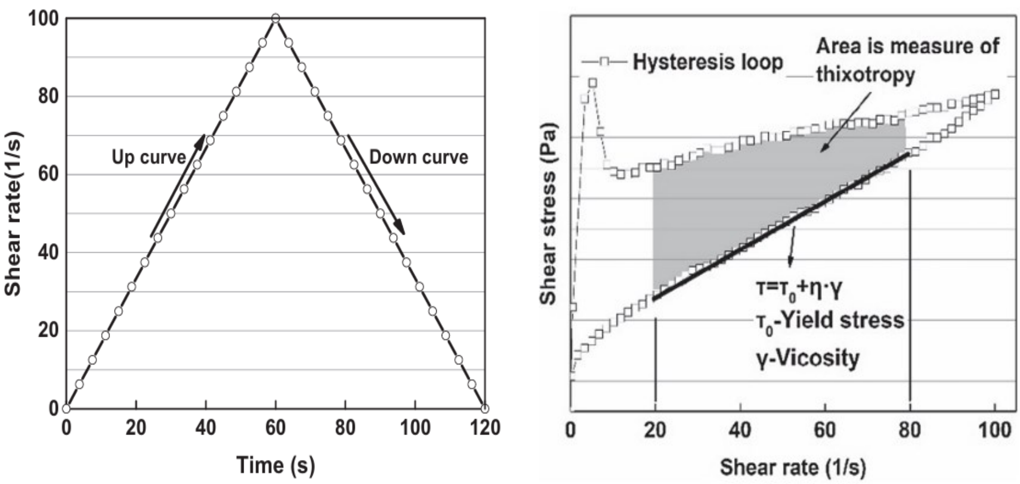

a) Loading history

b) typical result of a flow curve

Fig. 2. Loading history and typical result of a flow curve.

Table 2. Mixing procedure

Time (min)	Mixing Steps
0:00 – 1:00	Dry mix OPC, SCM, and aggregates at low speed.
1:00 – 2:00	Gradually add water, continue mixing at low speed.
2:00 – 3:00	Pause, scrape mixer sides, add superplasticizer, then resume at low speed.

3:00 – 4:00	Continue low-speed mixing.
4:00 – 4:30	Pause, scrape mixer sides again.
4:30 – 6:00	Mix at high speed.

3. Results

3.1 Overview of Rheological Behavior

This section discusses the rheological properties of six mortar mixes. These mixes were designed to investigate the effects of FA and SF on 3D-printable mortar. Flow curve data from a standard hysteresis loop test were used to evaluate key parameters such as static yield stress, dynamic yield stress, plastic viscosity, and thixotropy.

The static yield stress was identified as the highest point in the loading curve of the flow test. This point shows the stress needed to start flow. On the other hand, the dynamic yield stress was found at the intercept of the unloading curve with the shear stress axis. This indicates the stress needed to maintain flow. Plastic viscosity, which defines the flow rate under applied stress, was calculated from the linear section of the down-curve. Thixotropy was measured as the area between the up-curve and down-curve of the hysteresis loop. This shows how much energy is required to break down and rebuild the mix internal structure.

3.2 Flow curve for FA Mixes

Fig. 3 illustrates the hysteresis curves for the three mixes with varying FA proportions, tested at 0, 15, and 30 minutes resting times.

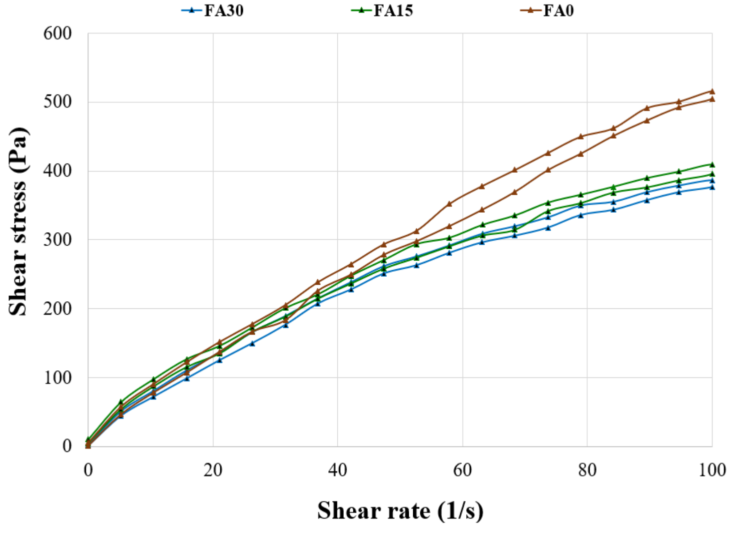

a) Resting time = 0 min

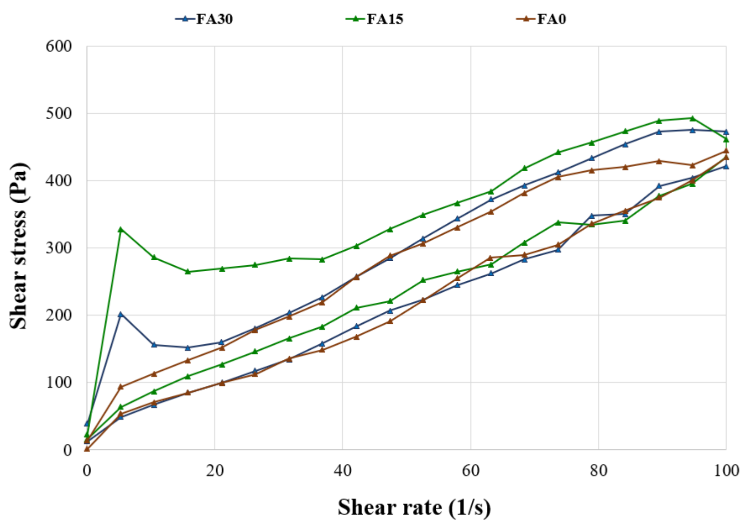

b) Resting time = 15 min

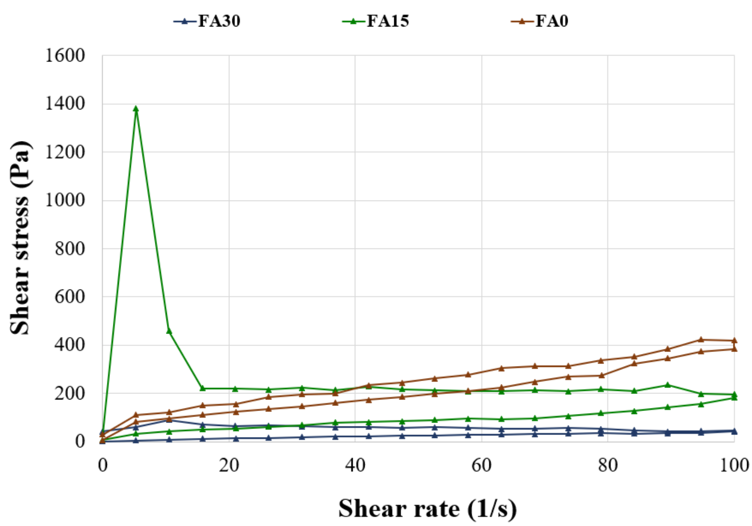

c) Resting time = 30 min

Fig. 3. Flow curves for FA mixes at different resting times.

The curves show a steady increase in shear stress as the shear rate rises for all mixes and resting times, indicating the material's growing resistance to flow as the rate of deformation increases. This behavior reflects the basic rheological response of the mortar, where higher shear rates demand more stress to break down the internal structure. The gradual changes in shear stress over the different resting times also shows how the mortar's flow properties evolve with time, as structural build-up and time-dependent rheological changes take place.

3.2.1 *Static and dynamic yield stresses*

As shown in Fig. 4, the static yield stress demonstrates varying trends across the resting times for the three mixes. For FA0, the static yield stress increases progressively with resting time, showing a steady rise from 0 to 15 minutes and continuing to increase at 30 minutes. FA15 exhibits the sharpest increase, with a significant rise between 15 and 30 minutes, resulting in the highest static yield stress among the three mixes at 30 minutes. For FA30, an unusual trend is observed. The static yield stress increases from 0 to 15 minutes but decreases noticeably at 30 minutes. This decline contrasts with the other mixes, highlighting a potential limitation in FA30's ability to maintain structural build-up at longer resting times.

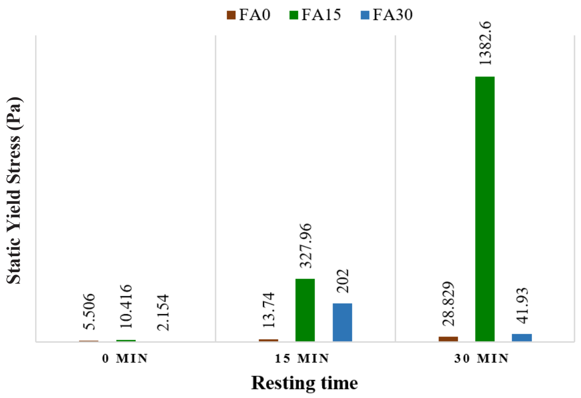

Fig. 4. Static stress for FA mixes at different resting times.

The dynamic yield stress results are presented in Fig. 5. FA0 shows a steady increase in dynamic yield stress with resting time, displaying consistent changes at each interval. FA15 experiences a steep rise between 0 and 15 minutes, followed by a smaller increase between 15 and 30 minutes, maintaining the highest values among the three mixes. FA30, however, shows the smallest dynamic yield stress values. It demonstrates only a slight increase between 0 and 15 minutes and then stabilizes with minimal change between 15 and 30 minutes. This limited development of dynamic yield stress suggests weaker resistance to flow under increasing shear compared to the other mixes.

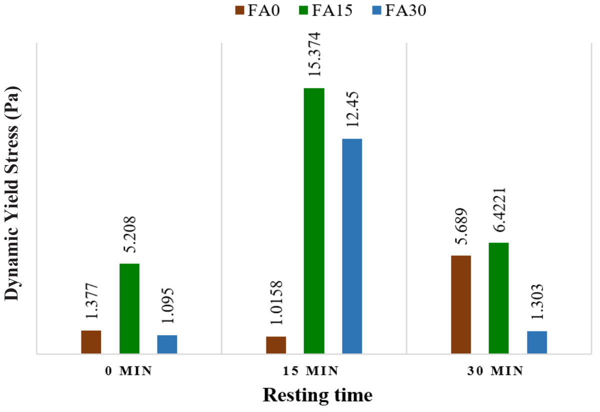

Fig. 5. Dynamic stress for FA mixes at different resting times.

3.2.2 *Thixotropy*

Fig. 6 shows the thixotropy trends for the three mixes over time. FA0 demonstrates a consistent increase in thixotropy with resting time, exhibiting moderate increases between each interval. FA15, however, shows a rapid rise, particularly between 15 and 30 minutes, leading to the highest thixotropy at 30 minutes. This indicates a strong time-dependent build-up of the internal structure for FA15. In contrast, FA30 exhibits the lowest thixotropy values across all resting times. Although an increase is observed between 0 and 15 minutes, the rate of increase slows considerably between 15 and 30 minutes, indicating a more limited structural development compared to FA0 and FA15.

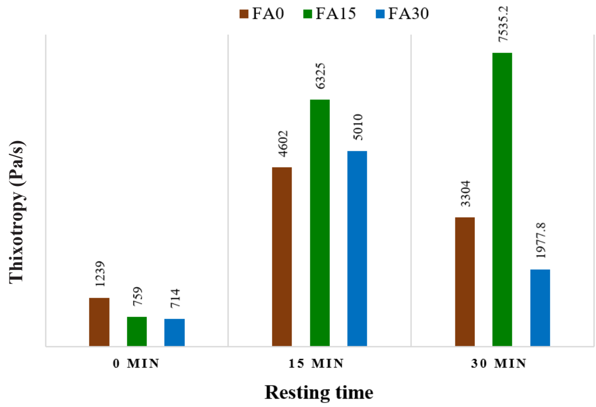

Fig. 6. Thixotropy for FA mixes at different resting times.

3.2.3 *Plastic Viscosity*

Fig. 7 highlights the trends in plastic viscosity for the FA mixes. FA0 begins with the highest viscosity at 0 minutes and shows a gradual decrease with time, exhibiting the lowest viscosity at 30 minutes. This suggests that FA0 becomes less resistant to flow over extended resting periods. FA15, on the other hand, shows an initial increase in viscosity from 0 to 15 minutes, reflecting the structural build-up over this period. After 15 minutes, the viscosity stabilizes with minimal change at 30 minutes. This stabilization suggests a balance between structural build-up and breakdown due to resting time. FA30 demonstrates consistently low viscosity values compared to the other mixes. A slight increase is observed from 0 to 15 minutes, followed by a significant drop at 30 minutes, indicating a reduction in its ability to resist deformation at higher resting times.

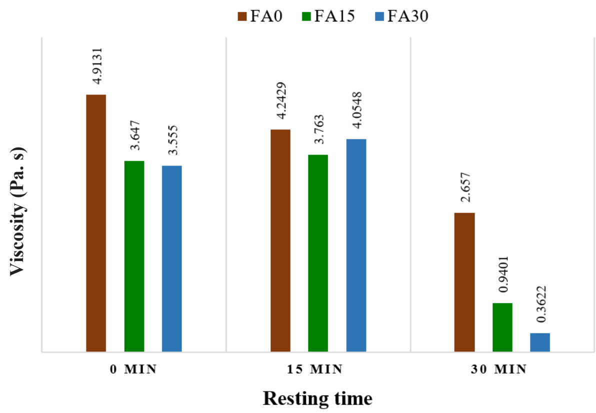

Fig. 7. Plastic viscosity for FA mixes at different resting times.

3.3 Flow curve for SF Mixes

Fig. 8 illustrates the hysteresis curves for the three mixes with varying SF proportions, tested at 0, 15, and 30 minutes resting times.

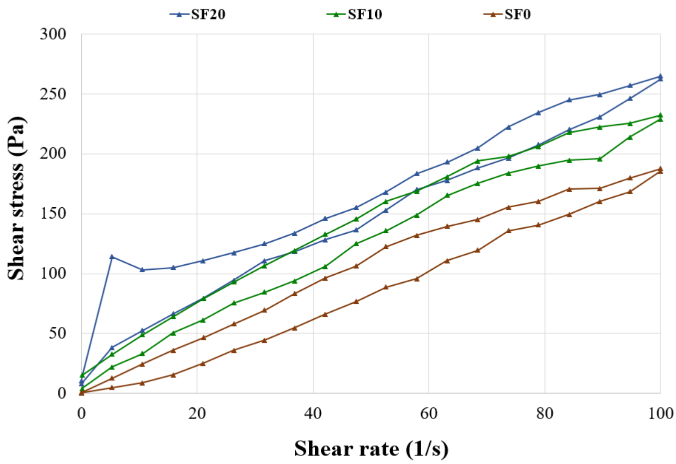

a) Resting time = 0 min

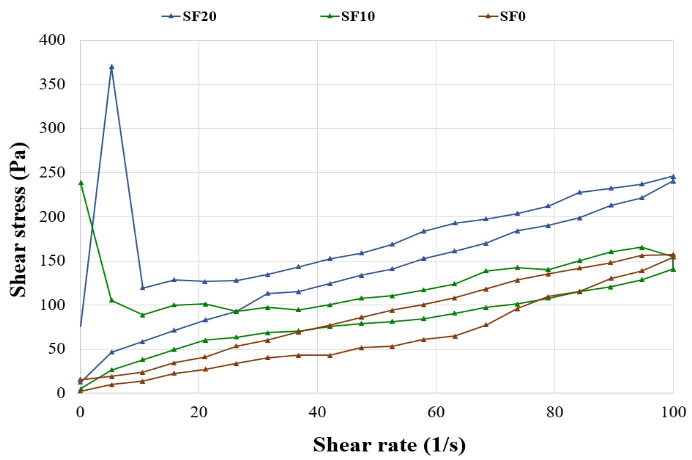

b) Resting time = 15 min

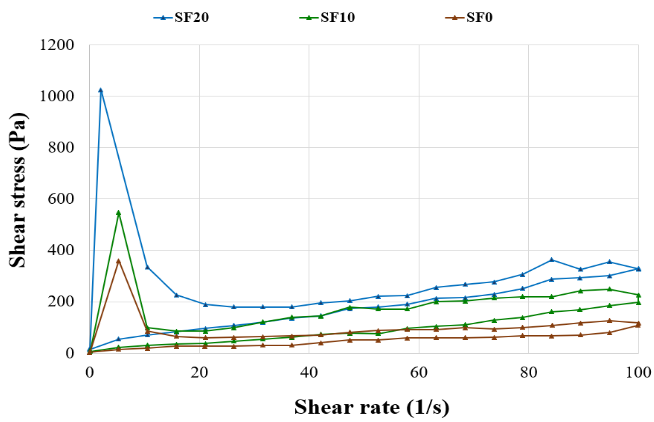

c) Resting time = 30 min

Fig. 8. Flow curves for SF mixes at different resting times.

The curves show a steady increase in shear stress with shear rate for all mixes and resting times. This indicates how the mortar resists deformation under different flow conditions. This behavior reflects the basic flow properties of the mortar. Higher shear rates require more stress to keep the flow going. The upward shifts in the curves over the three resting times point out the time-dependent changes in the mortar's structure, which are affected by resting time and SF content. At 0 minutes, the curves show fairly consistent patterns, demonstrating the initial flow characteristics of the mixes. At 15 minutes, the upward shift in the curves becomes more noticeable, reflecting the increasing resistance to flow as the internal structure continues to develop. By 30 minutes, the differences between the mixes are even more pronounced, with the curves shifting further upward across all shear rates. This shows a notable increase in the material's resistance to flow over time, influenced by the addition of SF and the longer resting period. These changes highlight how SF content and resting time affect the changing flow behavior of the mortar.

3.3.1 *Static and dynamic yield stresses*

The static yield stress of the SF mixes in Fig. 9 changed noticeably with different resting times, as seen in the figure. At 0 minutes, SF20 had the highest static yield stress compared to SF10 and SF0, which were much lower. By 15 minutes, all mixes showed an increase in static yield stress. SF20 had the largest rise, followed by SF10 and SF0. At 30 minutes, static yield stress continued to increase for all mixes, with SF20 reaching the highest value, well above SF10 and SF0. This trend demonstrates the growing resistance to flow over time, which is more evident as the SF content increases.

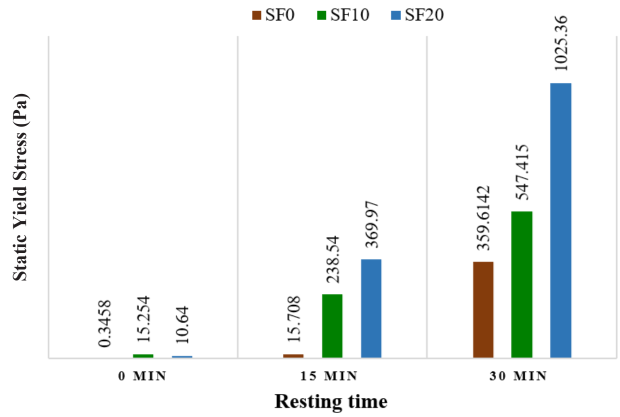

Fig. 9. Static stress for SF mixes at different resting times.

The dynamic yield stress shows significant variation across resting times, as depicted in Fig. 10. At 0 minutes, SF20 demonstrates the highest dynamic yield stress, followed by SF10, with SF0 showing the lowest value. By 15 minutes, all mixes experience an increase in dynamic yield stress. SF20 continues to exhibit the highest value, with a noticeable rise compared to SF10 and SF0, which also increase but to a lesser extent. At 30 minutes, the dynamic yield stress further increases for all mixes, with SF20 maintaining the highest value, significantly surpassing both SF10 and SF0.

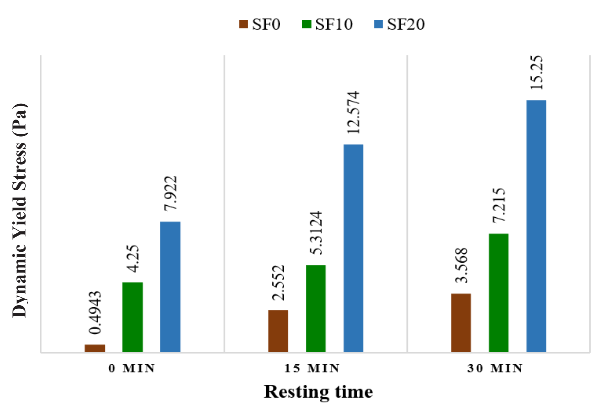

Fig. 10. Dynamic stress for SF mixes at different resting times.

3.3.2 *Thixotropy*

The thixotropy values of the SF mixes demonstrated notable variations over different resting times, as shown in Fig. 11. At 0 minutes, SF0 exhibited the highest thixotropy, followed by SF10 and SF20, which showed lower but comparable values. By 15 min, thixotropy increased slightly for all mixes, with SF0 and SF10 showing nearly identical values, while SF20 remained lower in comparison. At 30 minutes, significant differences observed, with SF10 demonstrating a substantial increase and reaching the highest value, far exceeding SF20 and SF0. SF20 also experienced a noticeable increase at 30 minutes, while SF0 showed only a marginal rise. These results indicate that resting time and SF content have a considerable influence on the thixotropy of the mixes, particularly at longer resting periods.

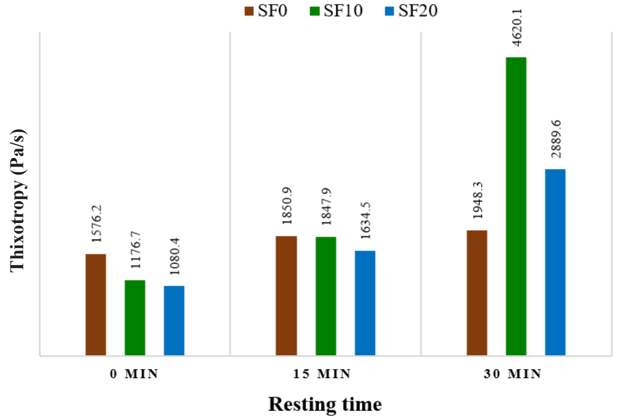

Fig. 11. Thixotropy for SF mixes at different resting times.

3.3.3 *Plastic Viscosity*

Fig. 12 highlights the trends in plastic viscosity for the mixes. At 0 minutes, all mixes exhibited relatively similar viscosity values, with SF10 having the highest value, followed closely by SF20 and SF0. By 15 minutes, SF20 displayed an increase in viscosity, becoming the highest among the mixes, while SF10 and SF0 both decreased, with SF0 recording the lowest viscosity at this time. At 30 minutes, SF20 exhibited a significant rise, reaching the highest viscosity value overall, followed by SF10, which also increased slightly. SF0, however, showed a further decrease and remained the lowest among the mixes.

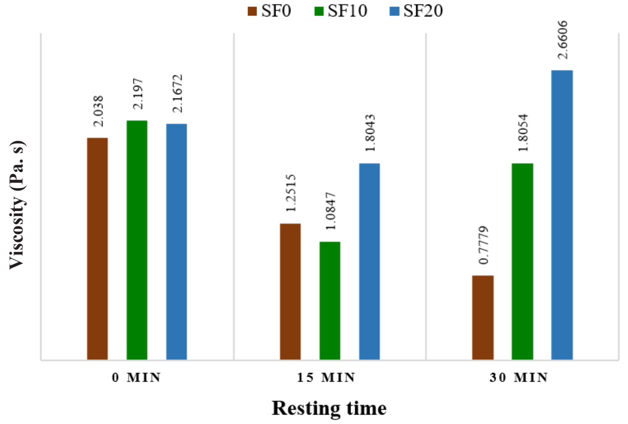

Fig. 12. Viscosity for SF mixes at different resting times.

4. Discussion

4.1 Static and Dynamic Yield Stresses

The static and dynamic yield stresses of the FA mixes (FA0, FA15, and FA30) and SF mixes (SF0, SF10, and SF20) showed significant changes over time. This reflected the impact of the material content and hydration processes.
The static and dynamic yield stresses of the FA mixes (FA0, FA15, and FA30) and SF mixes (SF0, SF10, and SF20) changed significantly over time because of material content and hydration processes. For the FA mixes, FA15 had the highest static and dynamic yield stresses at all resting times, with increases of about 85% compared to FA0. This is likely due to a balance between pozzolanic activity, the filler effect, and particle cohesion. Together, they help improve structural build-up. In contrast, FA30 showed a different trend. Its static yield stress increased at 15 minutes but dropped by over 70% at 30 minutes. This drop may be caused by the higher water demand of FA30. As a result, its internal structure weakens over time. The slower pozzolanic reaction may also contribute to this behavior. The result is reduced interparticle cohesion. Further investigation is needed to understand the mechanisms behind this unusual behavior and to explore possible solutions for improving the stability of FA30 mixes. FA0 consistently showed the lowest static and dynamic yield stresses, which highlights the lack of SCM contributions to structural development. For SF mixes, SF20 showed the highest static and dynamic yield stresses. By 30 minutes, it increased by more than 50% compared to SF10 and over 180% compared to SF0. This is due to the high reactivity and fine particles of silica fume. These properties increase the fast formation of calcium-silicate-hydrate (C-S-H) gel and create a denser particle network. SF10 showed moderate increases over time. At 30 minutes, its static and dynamic yield stresses were about 40% higher than SF0. For SF0, it consistently had the lowest static and dynamic yield stresses, showing it lacked reactive materials needed for hydration and structural build-up.

4.2 Thixotropy

Thixotropy trends for both FA and SF mixes demonstrated the time-dependent evolution of structural build-up and breakdown, influenced by material composition and hydration.

For the FA mixes, FA15 exhibited the highest thixotropy at 30 minutes, with approximately a 20% increase compared to FA30 and over 125% higher than FA0. This reflects its ability to recover its internal structure after shearing due to balanced pozzolanic activity and particle packing. At 15 minutes, FA15 displayed significant structural build-up, with about 37% higher thixotropy compared to FA0 and 26% higher than FA30. By 30 minutes, both FA0 and FA30 showed declines in thixotropy, with FA30 experiencing a reduction of nearly 60% compared to its peak at 15 minutes. This sharp drop in FA30 is attributed to its high-water demand and delayed pozzolanic reaction, which weakens the structure and prevents efficient recovery after shear. FA0's lower thixotropy reflects its reliance on the cement matrix without the benefits of supplementary pozzolanic activity.

For SF mixes, SF10 exhibited the highest thixotropy at 30 minutes, with approximately 60% higher values compared to SF20 and more than double the thixotropy of SF0. SF10's higher thixotropy suggests an optimal balance between particle cohesion and dispersibility, enabling better recovery of the internal structure. SF20, while having higher yield stresses, showed lower thixotropy at 30 minutes, likely due to over-consolidation caused by excessive SF, which limits structural rebuilding after shear. SF0 had the lowest thixotropy values throughout, reflecting its limited cohesion and structural development in the absence of SF.

4.3 Plastic viscosity

The plastic viscosity trends for both FA and SF mixes reveal complex behaviors influenced by hydration, particle interactions, and water availability. While viscosity generally increases over time due to structural build-up and densification, certain mixes exhibit decreases in viscosity at later stages, reflecting shear thinning and changes in microstructure.

For the FA mixes, FA0 initially exhibited the highest viscosity at 0 minutes, approximately 85% higher than FA30, as flow resistance was primarily governed by the cement matrix. However, its viscosity decreased steadily by about 45% at 30 minutes, indicating the inability of the cement matrix alone to sustain structural integrity during prolonged resting. FA15 showed stable viscosity at 15 minutes, maintaining about 30% higher viscosity than FA30, but a sharp reduction of nearly 75% at 30 minutes suggests the breakdown of flocculated structures formed earlier. This reduction is due to shear thinning, where hydration products, such as C-S-H gels, initially enhance interparticle cohesion but lose their structural effectiveness under prolonged shear or insufficient water retention. FA30 exhibited the lowest viscosity at 30 minutes, approximately 60% lower than its initial value, reflecting the impact of its high FA content. The slower pozzolanic reaction, combined with excessive water demand, diluted the mix, reduced interparticle friction, and hindered the formation of a cohesive microstructure.

For SF mixes, SF20 showed a steady rise in viscosity over time. At 30 minutes, its viscosity was about 50% higher than SF0. This is due to the high surface area and strong pozzolanic activity of SF. These properties help densify the structure and strengthen particle cohesion. SF10 had a moderate increase as its viscosity was about 30% higher than SF0 after 30 minutes. This suggests a good balance between workability and structural build-up, with enough water for hydration. In contrast, SF0 showed a steady drop in viscosity. Over 30 minutes, it decreased by nearly 60%. This drop reflects the lack of reactive SF, which limits densification and weakens particle cohesion. As a result, the mix becomes more fluid over time.

The drop in viscosity seen in FA15, FA30, and SF0 is due to hydration, flocculation, and water availability. As resting time increases, hydration products like C-S-H gels form and build structure, raising viscosity. But when mixes have few reactive materials or too much water, like FA30 and SF0, hydration becomes less effective. This weakens the internal structure and lowers viscosity. Shear thinning also affects the behavior as flocculated networks formed early break down under shear. In FA30, the slow pozzolanic reaction and high-water demand make the viscosity drops faster.

Similar results have been seen in previous research. When there is too much water or not enough reactive material, the viscosity drops over time because the structure doesn't build up properly during rest. For example, Roussel et al. [27] found that mixes with high amounts of supplementary cementitious materials delayed the development of the internal structure. Jayathilakage et al. [28] also highlighted the need to carefully balance water and binder to keep viscosity stable during 3D printing. These studies point to the importance of improving mix designs to avoid large drops in viscosity and ensure stable structures over time.

5. Conclusion

The results of this study show that different amounts of fly ash and silica fume can greatly impact yield stresses, viscosity, and thixotropy in 3D-printable mortars. Finding the right balance of these materials is important for maintaining workability and strong structural build up over time. The main observations are as follows:

- Moderately increasing fly ash content (FA15) enhanced both static and dynamic yield stresses and resulted in the highest thixotropy at longer resting times, indicating an optimal balance between workability and structural build-up.
- Excessive fly ash content (FA30) showed an unusual drop in yield stress after 30 minutes. This requires further investigation into the hydration process for this specific mixture.
- Higher silica fume content (SF20) led to pronounced increases in yield stresses and viscosity, demonstrating rapid formation of C-S-H gels and consolidated networks, beneficial for early structural gain in 3D printing.
- Despite SF20's superior yield stress, SF10 showed the highest thixotropy at 30 minutes, indicating that an intermediate silica fume dosage may offer the best compromise between flow and structural recovery post-shear.
- Select mixes (FA30, SF0) displayed a notable decrease in viscosity over time, attributed to interplay between hydration, water demand, and shear thinning, highlighting the need for balanced water-to-binder ratios to maintain rheological stability.
- Overall, a combination of moderate fly ash (around 15%) and intermediate silica fume (around 10%) shows promise in optimizing pumpability, extrudability, and layer stability in 3D-printable mortars, while excessive dosage of either SCM risks adverse effects on workability or final build strength.

The findings of this study are part of ongoing research to develop optimized 3D-printable cementitious mixes. These results provide a foundation for achieving a balance between flowability and structural stability while addressing practical challenges in large-scale applications. Future studies should investigate the long-term effects of hydration kinetics on the rheological behavior of 3D-printed mortars, particularly the synergy between fly ash and silica fume in enhancing structural build-up. Additionally, exploring durability and mechanical performance under real-world environmental conditions will be critical for scaling this technology to industrial applications. Further work will focus on ensuring the scalability and durability of these mixes in real-world construction scenarios.

Acknowledgement

The authors would like to thank the SCMAS research group at the Department of Civil and Environmental Engineering, University of Sharjah, for their support and guidance during this work. Their assistance and encouragement have been greatly appreciated.

References

1. B. Khoshnevis, Automated construction by contour crafting related robotics and information technologies, Autom. Constr. 13, 5–19 (2004)
2. R.A. Buswell, W.R. Leal de Silva, S.Z. Jones, J. Dirrenberger, 3D printing using concrete extrusion: A roadmap for research, Cem. Concr. Res. 112, 37–49 (2018)
3. M.T. Junaid, A. Shweiki, S. Barakat, M. Alhalabi, O. Mostafa, Flexural characterization and ductility assessment of small-scale mortar beams reinforced with 3D-printed polymers, Struct. 45, 1751–1761 (2022). https://doi.org/10.1016/j.istruc.2022.10.007
4. M.T. Junaid, M. Alhalabi, O. Mostafa, S. Barakat, Flexural characterization of concrete beams reinforced with 3D-printed formworks, Mater. Sci. Forum 1108, 181–189 (2023). https://doi.org/10.4028/p-D9r7Sj
5. P.F.G. Banfill, Rheology of fresh cement and concrete, Rheol. Rev. 1994, 61–130 (1994)
6. A.I. Laskar, S. Talukdar, Rheology of fly-ash-based geopolymer concrete, AEI 2008 (2008)
7. B. Panda, M.J. Tan, Rheological behavior of high volume fly ash mixtures containing micro silica for digital construction application, Constr. Build. Mater. 162, 286–294 (2019)
8. W. Xu, Y. Zheng, K. Wu, P. Feng, Y. Yao, Rheology, printability and buildability of 3D printed fly ash cementitious materials: Effect of fly ash and slump-retaining admixture, Cem. Concr. Compos. 126, 104352 (2022)
9. C.F. Ferraris, F.D. Larrard, N. Martys, Fresh concrete rheology: Recent developments, in Materials Science of Concrete VI, 215–241 (2001)
10. Y. Zhang, Y. Zhang, J. Pan, M.J. Tan, Printability region of building scale extruded concrete, Autom. Constr. 95, 263–272 (2018)
11. R.S. Ahari, T.K. Erdem, I. Koc, An experimental and numerical study on the effect of silica fume on fresh properties of self-compacting concrete, Comput. Concr. 15, 399–420 (2015)
12. D. Jiao, Z. Shui, Y. Huang, W. Chen, Effects of superfine cement on the fluidity and compressive strength of cement–silica fume paste, Mater. Struct. 50, 11 (2017)
13. M.A. Moeini, M.J. Tan, A. Perrot, FDM-based discrete element modelling of 3D concrete printing: From flow to filament bonding, Addit. Manuf. 36, 101452 (2020)
14. N. Roussel, Rheological requirements for printable concretes, Cem. Concr. Res. 112, 76–85 (2018)
15. L. Reiter, T. Wangler, N. Roussel, R.J. Flatt, Setting on demand for concrete extrusion, Cem. Concr. Res. 112, 86–95 (2018)
16. A.V. Rahul, M. Santhanam, H. Meena, Z. Ghani, 3D printable concrete: Mixture design and test methods, Cem. Concr. Compos. 97, 13–23 (2019)
17. M. Jalal, M. Fathi, M. Sharifipour, Effects of fly ash and slag on the mechanical properties, porosity and durability of concrete, Int. J. Civ. Eng. 13, 23–31 (2015)
18. G. Şahin, K.R. Akça, H. Yalçiner, Influence of silica fume on the rheological properties and buildability of 3D printable concrete, J. Mater. Civ. Eng. (in press) (2024)
19. R. Guo, C. Shi, Z. Wang, J. Xiao, On the rheology of 3D printable cementitious materials: Effect of curing and structural build-up, Constr. Build. Mater. 241, 118044 (2020)
20. B. Khoshnevis, Automated construction by contour crafting related robotics and information technologies, Autom. Constr. 13, 5–19 (2004). https://doi.org/10.1016/S0926-5805(03)00039-X
21. R.A. Buswell, W.R. Leal de Silva, S.Z. Jones, J. Dirrenberger, 3D printing using concrete extrusion: A roadmap for research, Cem. Concr. Res. 112, 37–49 (2018). https://doi.org/10.1016/j.cemconres.2018.06.001
22. C. Gonzalez-Gomez, I. MacLeod, G.J. Gibbons, A critical review of 3D printing in construction: Benefits, challenges, and risks, J. Mater. Sci. 56, 12967–12984 (2021). https://doi.org/10.1007/s43452-020-00038-w
23. R. Jayathilakage, P. Rajeev, J.G. Sanjayan, Challenges and limitations of 3D construction printing, Cem. Concr. Compos. 120, 104064 (2021). https://doi.org/10.1016/j.cemconcomp.2021.104064
24. A. Perrot, D. Rangeard, E. Courteille, Review of rheology in cement-based materials and its application to 3D printing, Rheol. J. 51, 1–10 (2020). https://doi.org/10.1007/s11340-020-00701-w
25. Y. Zhang, Y. Zhang, J. Pan, M.J. Tan, Interlayer bonding investigation of 3D printing cementitious materials with fluidity retaining polycarboxylate superplasticizer and high dispersion polycarboxylate superplasticizer, Constr. Build. Mater. 327, 126963 (2022). https://doi.org/10.1016/j.conbuildmat.2022.126963
26. Y. Zhang, Y. Zhang, G. Liu, Y. Yang, M. Wu, B. Pang, Fresh properties of a novel 3D printing concrete ink, Constr. Build. Mater. 174, 263–271 (2018). https://doi.org/10.1016/j.conbuildmat.2018.04.115
27. N. Roussel, C. Stefani, R. Leroy, From mini-cone test to Abrams cone test: Measurement of cement-based materials yield stress using slump tests, Cem. Concr. Res. 40, 1517–1521 (2010). https://doi.org/10.1016/j.cemconres.2010.11.006
28. R. Jayathilakage, P. Rajeev, J.G. Sanjayan, Yield stress criteria to assess the buildability of 3D concrete printing, Cem. Concr. Compos. 120, 104064 (2021). https://doi.org/10.1016/j.cemconcomp.2021.104064